

De Novo Mutations in *SLC25A24* Cause a Craniosynostosis Syndrome with Hypertrichosis, Progeroid Appearance, and Mitochondrial Dysfunction

Nadja Ehmke,^{1,2,3,*} Luitgard Graul-Neumann,¹ Lukasz Smorag,⁴ Rainer Koenig,⁵ Lara Segebrecht,¹ Pilar Magoulas,^{6,7} Fernando Scaglia,^{6,7} Esra Kilic,⁸ Anna F. Hennig,^{1,9} Nicolai Adolphs,¹⁰ Namrata Saha,^{1,3,11,12} Beatrix Fauler,¹³ Vera M. Kalscheuer,³ Friederike Hennig,³ Janine Altmüller,^{14,15} Christian Netzer,¹⁶ Holger Thiele,¹⁴ Peter Nürnberg,^{14,15,17} Gökhan Yigit,⁴ Marten Jäger,¹⁸ Jochen Hecht,^{19,20} Ulrike Krüger,¹⁸ Thorsten Mielke,¹³ Peter M. Krawitz,^{1,3,9} Denise Horn,¹ Markus Schuelke,²¹ Stefan Mundlos,^{1,3,9} Carlos A. Bacino,^{6,7} Penelope E. Bonnen,⁶ Bernd Wollnik,⁴ Björn Fischer-Zirnsak,^{1,3,9,22} and Uwe Kornak^{1,3,9,22,*}

Gorlin-Chaudhry-Moss syndrome (GCMS) is a dysmorphic syndrome characterized by coronal craniosynostosis and severe midface hypoplasia, body and facial hypertrichosis, microphthalmia, short stature, and short distal phalanges. Variable lipoatrophy and cutis laxa are the basis for a progeroid appearance. Using exome and genome sequencing, we identified the recurrent *de novo* mutations c.650G>A (p.Arg217His) and c.649C>T (p.Arg217Cys) in *SLC25A24* in five unrelated girls diagnosed with GCMS. Two of the girls had pronounced neonatal progeroid features and were initially diagnosed with Wiedemann-Rautenstrauch syndrome. *SLC25A24* encodes a mitochondrial inner membrane ATP-Mg/P_i carrier. In fibroblasts from affected individuals, the mutated *SLC25A24* showed normal stability. In contrast to control cells, the probands' cells showed mitochondrial swelling, which was exacerbated upon treatment with hydrogen peroxide (H₂O₂). The same effect was observed after overexpression of the mutant cDNA. Under normal culture conditions, the mitochondrial membrane potential of the probands' fibroblasts was intact, whereas ATP content in the mitochondrial matrix was lower than that in control cells. However, upon H₂O₂ exposure, the membrane potential was significantly elevated in cells harboring the mutated *SLC25A24*. No reduction of mitochondrial DNA copy number was observed. These findings demonstrate that mitochondrial dysfunction with increased sensitivity to oxidative stress is due to the *SLC25A24* mutations. Our results suggest that the *SLC25A24* mutations induce a gain of pathological function and link mitochondrial ATP-Mg/P_i transport to the development of skeletal and connective tissue.

Gorlin-Chaudhry-Moss syndrome (GCMS [MIM: 233500]) is a rare condition with a distinctive facial gestalt due to coronal craniosynostosis, maxillary hypoplasia, and microphthalmia leading to narrow palpebral fissures.¹ Other core features include coarse scalp hair and generalized hypertrichosis, severe hypermetropia, short stature, short distal phalanges, dental anomalies, and genital hypoplasia. Several individuals present with translucent or loose skin and reduced subcutaneous adipose tissue, leading to a progeroid appearance.² Psychomotor development can be delayed, but intelligence is usually in the normal range. The syndrome was first described in 1960 by Gorlin, Chaudhry, and Moss in two sisters.¹ Since then,

only six further individuals with suggested GCMS (one pair of siblings and one individual with mild GCMS manifestations that more resemble Saethre-Chotzen syndrome [MIM: 101400]³) have been published.^{2,4–6} Most authors have supposed an autosomal-recessive mode of inheritance,^{1,4,7} but because all reported individuals are female, X-linked dominant inheritance with male lethality and germline mosaicism (in the case of the sisters with GCMS) have also been considered.^{2,6} Several authors have pointed out the phenotypic overlap between GCMS and Petty-type congenital progeroid syndrome (MIM: 612289),^{2,6,8} emphasizing the progeroid aspect of GCMS.

¹Institute of Medical and Human Genetics, Charité – Universitätsmedizin Berlin, 13353 Berlin, Germany; ²Berlin Institute of Health, 10117 Berlin, Germany; ³Max Planck Institute for Molecular Genetics, Development and Disease Group, 14195 Berlin, Germany; ⁴Institut für Humangenetik, Universitätsmedizin Göttingen, 37073 Göttingen, Germany; ⁵Institute of Human Genetics, Goethe University Frankfurt, 60590 Frankfurt am Main, Germany; ⁶Department of Molecular and Human Genetics, Baylor College of Medicine, Houston, TX 77030, USA; ⁷Texas Children's Hospital, Houston, TX 77030, USA; ⁸Pediatric Genetics, Pediatric Hematology Oncology Research & Training Hospital, 06110 Ankara, Turkey; ⁹Berlin-Brandenburg Center for Regenerative Therapies, Charité – Universitätsmedizin Berlin, 13353 Berlin, Germany; ¹⁰Department of Craniomaxillofacial Surgery, Charité – Universitätsmedizin Berlin, 13353 Berlin, Germany; ¹¹Berlin-Brandenburg School for Regenerative Therapies, Charité – Universitätsmedizin Berlin, 13353 Berlin, Germany; ¹²Max Planck International Research Network on Aging, 18057 Rostock, Germany; ¹³Max Planck Institute for Molecular Genetics, Microscopy and Cryo-electron Microscopy Group, 14195 Berlin, Germany; ¹⁴Cologne Center for Genomics, University of Cologne, 50931 Cologne, Germany; ¹⁵Center for Molecular Medicine Cologne, University of Cologne, 50931 Cologne, Germany; ¹⁶Institute of Human Genetics, University Hospital Cologne, 50931 Cologne, Germany; ¹⁷Cologne Excellence Cluster on Cellular Stress Responses in Aging-Associated Diseases, University of Cologne, 50674 Cologne, Germany; ¹⁸Genomics Core Facility, Campus Virchow Klinikum, Berlin Institute of Health, 13353 Berlin, Germany; ¹⁹Center for Genomic Regulation, Barcelona Institute for Science and Technology, Dr. Aiguader 88, 08003 Barcelona, Spain; ²⁰Universitat Pompeu Fabra, 08002 Barcelona, Spain; ²¹Department of Neuropediatrics and NeuroCure Clinical Research Center, Charité – Universitätsmedizin Berlin, 10117 Berlin, Germany

²²These authors contributed equally to this work

*Correspondence: nadja.ehmke@charite.de (N.E.), uwe.kornak@charite.de (U.K.)

<https://doi.org/10.1016/j.ajhg.2017.09.016>

© 2017 American Society of Human Genetics.

Table 1. Clinical Presentation and Genotype of the Five Individuals with GCMS and a Progeroid Appearance

	Individual 1	Individual 2⁵	Individual 3	Individual 4	Individual 5
Sex	female	female	female	female	female
Ethnicity	Polish	Hungarian	German	Turkish	northern European
Age at last exam	5.5 years	7 years	5 years	1.5 years	14 years
Result of SLC25A24 Analysis (GenBank: NM_013386)					
Mutation	c.650G>A (p.Arg217His)	c.650G>A (p.Arg217His)	c.650G>A (p.Arg217His)	c.650G>A (p.Arg217His)	c.649C>T (p.Arg217Cys)
Type	heterozygous, <i>de novo</i>	heterozygous, <i>de novo</i>	heterozygous, <i>de novo</i>	heterozygous, <i>de novo</i>	heterozygous, <i>de novo</i>
Clinical Manifestations (HPO Term)					
Birth weight	2,200 g (−2.4 SD)	2,225 g (−1 SD)	1,600 g (−1.1 SD)	1,700 g (−3.4 SD)	1,722 g (−2.6 SD)
HC at birth	28 cm (−4.2 SD)	unknown	29 cm (−3.4 SD)	29.4 cm (−3 SD)	unknown
IUGR (HP:0001511)	+	−	+	+	+
Postnatal short stature (HP:0004322)	+	−	+	+	+
Failure to thrive (HP:0001508)	+	+	+	+	+
Microcephaly (HP:0011451)	+	−	+	+	−
Coronal craniosynostosis (HP:0004440)	clinical	+	+	+	unknown
Brachycephaly (HP:0000248)	+	+	+	+	+
Large anterior fontanelle (HP:0000260)	+	−	+	+	−
Broad forehead (HP:0000337)	+	+	+	+	+
Depressed supraorbital ridge (HP:0009891)	+	+	+	+	+
Midface hypoplasia (HP:0011800)	+	+	+	+	+
Prognathia or tongue protrusion (HP:0000303)	+	+	+	+	+
Short and downslanting palpebral fissures (HP:0000494)	+	+	+	+	+
Microphthalmia (HP:0000568) or hyperopia (HP:0000540)	+	+	+	+	+
Eyelid anomalies (HP:0000492)	−	−	−	+	−
Low anterior and posterior hair line (HP:0009553)	+	+	+	+	+
Coarse scalp hair (HP:0002208)	+	+	−	+	+
Hypertrichosis (HP:0000998)	+	+	+	+	+
Wrinkled skin (HP:0007392)	+	+	+	+	+
Dermal translucency (HP:0010648)	+	−	+	+	+
Reduced subcutaneous fat tissue (HP:0001002)	+	−	+	+	+
Small nails (HP:0001792)	+	−	+	+	+
Short distal phalanges (HP:0009882)	−	−	+	+	+
Syndactyly (HP:0001159)	−	+	+	−	+

(Continued on next page)

Table 1. Continued

	Individual 1	Individual 2 ⁵	Individual 3	Individual 4	Individual 5
Hypoplastic labia majora (HP:0000059)	+	+	+	+	+
Oligodontia or microdontia (HP:0000691)	–	+	+	+	+
Highly arched (HP:0002705) or cleft (HP:0000175) palate	–	–	–	highly arched	–
Conductive hearing impairment (HP:0000405)	–	–	+	+	+
Low-set, dysplastic ears (HP:0000369)	–	+	+	+	+
Congenital heart disease (HP:0030681)	–	–	PDA, ASD II, PAH	hypertrophic left ventricle	PDA, PAH, TI
Aortic ectasia (HP:0001724)	unknown	unknown	+	–	+
Umbilical hernia (HP:0001537) or abdominal muscle hypoplasia (HP:0005243)	+	–	+	+	+
Other anomalies	small mouth	wound healing disorder	feeding via PEG tube, hemiplegia after craniocerebral injury, hydrocephalus communis, GER, prominent glabella	Dandy Walker malformation, bilateral urolithiasis	feeding via PEG tube, GER, constipation, hydrocephalus
Psychomotor development	delayed with normal outcome	normal	delayed speech development with normal outcome, delayed motor development due to muscle weakness	delayed with normal outcome	delayed motor development due to muscle weakness

Abbreviations are as follows: +, present; –, not present; ASD, atrial septal defect; GER, gastroesophageal reflux; HC, head circumference; IUGR, intrauterine growth restriction; PAH, pulmonary artery hypertension; PDA, persistent ductus arteriosus; PEG, percutaneous endoscopic gastrostomy; TI, tricuspid insufficiency.

In the present study, we evaluated five unrelated girls showing the typical hallmarks of GCMS (described above) (Table 1). Two of them (individuals 4 and 5) were initially diagnosed with Wiedemann-Rautenstrauch syndrome (MIM: 264090). Individual 2 was previously reported by Adolphs and coworkers.⁵ All but one of the five girls had oligo- and microdontia, and all had wrinkled skin and dystrophy either congenitally or in early infancy (Figure 1). Individuals 1, 4, and 5 had an umbilical hernia, whereas individual 3 additionally presented with hypoplasia of the abdominal wall muscles. Individuals 3 and 5 had severe failure to thrive, requiring feeding through a percutaneous endoscopic gastrostomy tube. The progeroid aspect was most pronounced in individuals 1 and 4. Individual 4 showed a distinct facial aspect, primarily due to the marked reduction of adipose tissue. Cranial MRI scans displayed a Dandy-Walker malformation in individual 4. The motor development of the five girls had been delayed as a result of muscular hypotonia, especially in individual 3, but was in the normal range when last examined. Individual 4 died at the age of 20 months from a urinary infection. A detailed phenotypic description of the five individuals is provided in the Supplemental Note.

The parents provided their written consent for genetic testing and the publication of images. Individuals of families 1 and 5 (proband and parents), individual 2, and individual 4 were subjected to exome or whole-genome sequencing after approval was obtained from the ethics board of the Charité – Universitätsmedizin Berlin, University Medical Center Göttingen, and Baylor College of Medicine. DNA from all individuals was extracted from peripheral-blood lymphocytes according to standard protocols. Targeted enrichment of the DNA samples of family 1 and individual 2 was performed with SureSelect All Exon Kit V2 (Agilent), and then the samples were sequenced on Illumina's HiSeq 1500 system. Sequence reads were mapped to the haploid human reference genome sequence (GRCh37, UCSC Genome Browser hg19) with the Burrows-Wheeler Aligner (BWA MEM).⁹ Single-nucleotide variants and short indels were called with the Genome Analysis Toolkit (GATK) according to the GATK Best Practices.^{10,11} The variant annotation on a functional level was performed with Jannovar, and GeneTalk was used for filtering and further data analysis.^{12,13} All variants with an allele frequency above 0.01 in healthy control individuals from large population studies were excluded.^{14,15} Filtering according to the autosomal-recessive model of inheritance



Figure 1. Facial and Body Photographs of Individuals 1–4 (I1–I4) at Different Ages Show the Clinical Features and Course of GCMS
 (A and F) Facial photographs of I1 at the age of 3.5 (A) and 5.5 (F) years. Note the turribrachycephaly, broad forehead, coarse parietal scalp hair, low anterior hair line, facial hypertrichosis, depressed supraorbital ridges, laterally upslanting eyebrows, severe midface hypoplasia, downslanting and short palpebral fissures, ocular proptosis, small mouth, thin upper lip, and protruding lower lip and tongue.
 (B and G) Front (B) and side (G) photographs of I3 at birth show brachycephaly, a broad forehead, a depressed nasal root, midface hypoplasia, short palpebral fissures, small, round, and dysplastic ears, and a median chin crease.
 (C) Frontal photograph of I3 at the age of 5 years after surgical correction of the fused coronal suture. Note the thick eyebrows, depressed supraorbital ridges with prominent glabella, deeply set eyes, depressed nasal bridge, short nose, long philtrum, thin upper lip, and prognathia.
 (D, E, and J) Front (D) and side (J) facial photographs of I4 at the age of 5 months and at 1.5 years (E). In addition to the aforementioned facial features, this individual showed arched eyebrows, hypertelorism, sagging skin, and sparse parietal scalp hair. The reduction of facial adipose tissue is more pronounced at the younger age.
 (H) Body photograph of I3 at the age of 5 years after surgical correction of the umbilical hernia shows thin, translucent skin, abdominal muscle hypoplasia, and a gastrostoma.
 (I) Body photograph of I4 at the age of 1.5 years shows a protruding abdomen, an umbilical hernia, translucent and wrinkled skin, and reduced subcutaneous adipose tissue.
 (K) Photograph of the back of I1 at the age of 5.5 years shows wrinkled skin, reduced adipose tissue, and hypertrichosis, especially in the lumbar region.
 (L and M) Hand photographs of I3 (L) and I4 (M) show wrinkled skin and small distal phalanges and fingernails.
 (N) Photograph of the right foot of I1 at the age of 5.5 years shows a hallux valgus and a small nail of the fifth toe.
 (O) Photograph of the right foot of I3 at the age of 5 years shows a sandal gap and cutaneous 2/3 and 4/5 syndactyly of the toes.

did not yield any candidate genes. Searching for potential *de novo* variants, we identified only one candidate gene: *SLC25A24* (GenBank: NM_013386.4; MIM: 608744). The missense variant c.650G>A (p.Arg217His) (chr1: g.108700103C>T [GRCh37]) in exon 5 occurred *de novo*

in individual 1 and was also detectable in individual 2 (Figure S1). We validated the variants in individuals 1 and 2 and verified the *de novo* occurrence of the variant in individual 2 by Sanger sequencing (all sequencing primers are available upon request). Subsequently, we

analyzed exon 5 of *SLC25A24* in family 3 by Sanger sequencing and found the same *de novo* variant (c.650G>A [p.Arg217His]) in individual 3. Independently, the DNA of individual 4 was analyzed with the SureSelect Human All Exon V6 enrichment kit and an Illumina HiSeq 4000 sequencer. The Varbank pipeline of the Cologne Center for Genomics was used for analysis of the exome data as previously described.^{16,17} The identified mutation in *SLC25A24* (c.650G>A [p.Arg217His]) was confirmed by Sanger sequencing, and its *de novo* occurrence was confirmed by Sanger sequencing of parental DNAs. Whole-genome shotgun sequencing was conducted on individual 5 and her parents with an Illumina HiSeq 2000. These data were analyzed according to previously described methods.^{18,19} The heterozygous *de novo* mutation c.649C>T (p.Arg217Cys) (chr1: g.108700104G>A [GRCh37]) in *SLC25A24* was identified (Figure S1). Parenthood was confirmed by SNP analysis of the next-generation sequencing data of families 1 and 5, as well as by single-tandem-repeat analysis in families 2–4.²⁰ The missense variants c.650G>A and c.649C>T were not found in the ExAC Browser, gnomAD, or 1000 Genomes.^{14,15} The variants were classified as disease causing by MutationTaster,²¹ damaging by SIFT,²² and probably damaging by PolyPhen-2²³ as a result of the evolutionary conservation of the arginine residue at position 217 (Figure 2A).

SLC25A24 encodes a mitochondrial inner membrane ATP-Mg/P_i carrier, also known as short Ca²⁺-binding mitochondrial carrier 1 (SCaMC1), which consists of an N-terminal calcium-binding domain (containing four EF-hand motifs) followed by six transmembrane helices and a short C terminus.²⁵ Arg217 is located at the end of the predicted helix 1 (H1) of the transmembrane domain (Figure 2A).²⁶ *SLC25A24* (UniProt: Q6NUK1) mediates an exchange of ATP-Mg²⁺ for HPO₄²⁻ depending on the presence of Ca²⁺ in the intermembrane space.^{27–29} Previous work indicated a role of *SLC25A24* in resistance to oxidative stress, given that knockdown of *SLC25A24* in cancer cells was associated with increased cell death and mitochondrial swelling after treatment with hydrogen peroxide (H₂O₂).³⁰ In order to examine the effect of the identified mutations, we cultured skin fibroblasts from individuals 1 and 4 according to standard procedures. We investigated *SLC25A24* mRNA levels by using cDNA sequencing and quantitative PCR. No changes in gene expression were found, indicating stability of the transcript harboring the mutation (Figure S1). Furthermore, immunoblot analysis using an anti-*SLC25A24* antibody (Sigma HPA028519) showed no alteration of *SLC25A24* levels in cells harboring the amino acid change p.Arg217His, indicating stability of the altered polypeptide (Figure 2B).

Under normal culture conditions, the probands' fibroblasts showed mitochondrial swelling, which developed into mitochondrial ballooning after treatment with 10 μM H₂O₂ for 1.5 hr (Figure 2C). H₂O₂ induces oxidative stress, to which mitochondria can respond by forming the

mitochondrial permeability transition pore (mPTP).³¹ To further investigate these effects, we transfected fibroblasts from individual 1 and control cells with a red fluorescent protein (RFP) targeted to the mitochondrial matrix via a COX8 targeting signal. Using live-cell imaging, we again found mitochondrial swelling in the mutant fibroblasts under normal culture conditions and after oxidative stress, whereas control fibroblasts appeared almost unchanged (Figure 2D; Movies S1 and S2). These findings were corroborated by transmission electron microscopy (TEM) (Figure 2E). Mitochondrial DNA (mtDNA) deletions and copy-number variations were excluded by long-range and quantitative PCR, respectively, as previously described (Figure S2).³²

We next wanted to investigate the influence of p.Arg217His on the subcellular localization of *SLC25A24*. We performed a crude enrichment of mitochondria from control and proband-derived fibroblasts as described previously.³³ We again found *SLC25A24* to be stable and exclusively present in the mitochondria-enriched fraction, indicating normal targeting to this organelle (Figure 3A). Additionally, we purchased a pDONR221 plasmid containing the *SLC25A24* open reading frame (ORF) from DNASU. The base-pair exchange c.650G>A was introduced by site-directed mutagenesis, and wild-type (WT) and mutant ORFs were cloned into a pEF5/FRT/V5 (Invitrogen) expression vector. Transient transfection of HeLa cells with the use of JetPei (PolyPlus) resulted in protein amounts similar to those of the intrinsic protein (Figure 3B). WT and mutant proteins both localized to mitochondria, indicating intact mitochondrial targeting. However, the transient expression of p.Arg217His *SLC25A24* caused mitochondrial swelling and increased fragmentation, whereas mitochondria in cells overexpressing WT *SLC25A24* remained unchanged. Upon treatment with H₂O₂, the impact on the mitochondrial structure was even more pronounced in cells overexpressing the mutant than in the probands' fibroblasts (Figure 3C).

Furthermore, we monitored the mitochondrial membrane potential (MMP). 24 hr after seeding, fibroblasts were loaded with JC-1 (1 μg/mL; Molecular Probes), a ratio-metric dye commonly used for monitoring the MMP. After 20 min of loading, the fluorescence was measured at 550 and 580 nm with a GloMax Discover System (Promega), and the ratios of the intensities were compared. Under normal culture conditions, we observed no abnormality of the MMP in the probands' fibroblasts (Figure 4A). However, after treatment with H₂O₂, the MMP appeared higher in fibroblasts harboring the mutant *SLC25A24* than in control cells, indicating an altered proton gradient (Figure 4B).

Given the proposed function of *SLC25A24*, we were also interested in the ATP content of the mitochondrial matrix. Therefore, we targeted firefly luciferase, an ATP-dependent enzyme, to this compartment by N-terminal fusion with a COX8 targeting signal. Using the Amaxa system, we transfected control and proband-derived fibroblasts with these

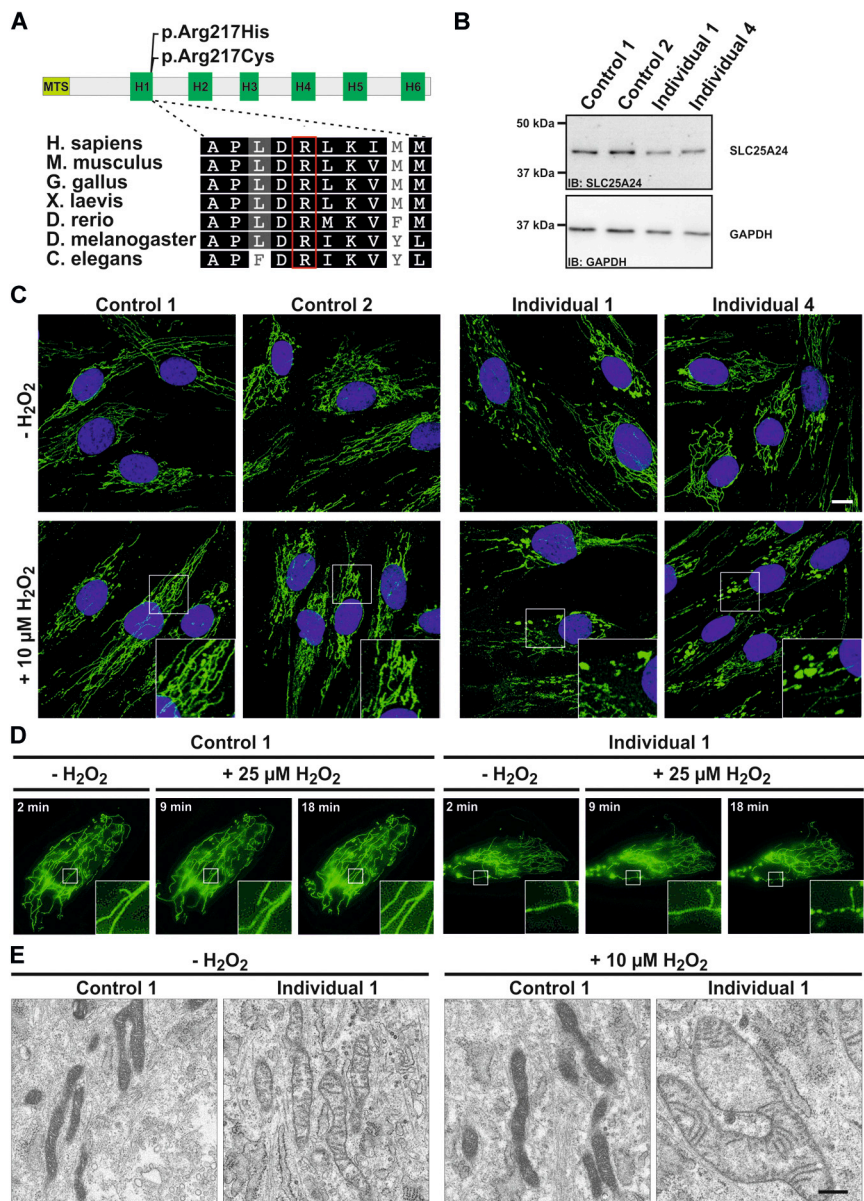


Figure 2. Cellular Alteration in Fibroblasts Carrying p.Arg217His

(A) Schematic overview of the SLC25A24 primary structure. The protein contains a predicted N-terminal mitochondrial targeting signal (MTS). The six known transmembrane helices (H1–H6) are depicted. The amino acid changes p.Arg217His and p.Arg217Cys localize at the end of H1. Interspecies comparison of the C-terminal end of H1 shows a high conservation down to *C. elegans*, including Arg217.

(B) In this and other experiments, control fibroblasts were obtained from healthy individuals aged 20–26 years and compared with fibroblasts from individuals 1 and 4. For immunoblotting (IB), cells were lysed with modified RIPA (50 mM Tris-HCL, 1% NP40, 0.25% Na-deoxycholat, 150 mM NaCl, and 1 mM EDTA + Complete Protease Inhibitor Cocktail [Roche]), and protein concentrations were determined with the BCA-Kit (Pierce). A total amount of 5 μg protein was separated on a SDS-PAGE gel, and proteins were transferred to nitrocellulose membranes. Membranes were blocked for 30 min at room temperature (RT), and primary antibodies (SLC25A24, Sigma; GAPDH, Ambion) were incubated overnight at 4°C. After washing, the corresponding horseradish-peroxidase-conjugated secondary antibodies were incubated for 1 hr at RT. Bands were visualized with ECL reagent (PerkinElmer). Immunoblot analysis of lysates from control and proband-derived skin fibroblasts revealed no alterations of SLC25A24 levels. This experiment was performed three times with different cell lysates.

(C) Immunofluorescence staining of fibroblasts under normal culture conditions and treated with 10 μM H₂O₂ for 1.5 hr. Cells grown on glass coverslips were washed three times in phosphate-buffered saline (PBS), fixed for 10 min at 4°C in 4% paraformaldehyde, and permeabilized with 0.4% Triton X-100 in 3% BSA in 1× PBS for 10 min. To visualize the mitochondrial

network, we used mouse anti-cyclophilin F (Abcam). Secondary antibody was anti-mouse IgG Alexa Fluor 488 (Invitrogen, Molecular Probes). DNA was stained by DAPI, and cells were mounted in Fluoromount G. This experiment was performed four times. Both controls showed reticular mitochondrial morphology, whereas the cells harboring p.Arg217His mitochondria were swollen. Scale bar, 10 μm.

(D) Live fibroblasts from control 1 and individual 1 transfected with a RFP targeted to mitochondria were imaged under normal culture conditions and showed an intact reticular network and some abnormally shaped mitochondria in the proband's cells. After treatment with 25 μM H₂O₂, an increased swelling of mitochondria was detectable in the fibroblasts from the affected individual 1. The complete experiment is shown in [Movies S1](#) and [S2](#). This experiment was performed twice.

(E) Transmission electron micrographs from control and proband-derived fibroblasts. For TEM analysis, cells grown on Thermanox plastic coverslips (Nunc, Thermo Fischer) were cultivated under normal culture conditions and in culture medium supplemented with 10 μM H₂O₂ for 1.5 hr. Cells were fixed with 2.5% glutaraldehyde (Sigma) and processed for TEM as described previously.²⁴ Imaging was performed with a Tecnai Spirit transmission electron microscope (FEI) equipped with a 4kx4k F416 CMOS camera (TVIPS) and operated at 120 kV. Under both conditions, control cells showed morphologically unaffected mitochondria. Under normal culture conditions, the cells of individual 1 showed slightly swollen mitochondria. After treatment with H₂O₂, this effect became aggravated. Scale bar, 0.5 μm.

constructs and a cytoplasmic *Renilla*-expressing plasmid. Cells were loaded with the *in vivo* substrates ViviRen (*Renilla*) and VivoGlo (firefly) from Promega. The luciferase signal intensities were collected with the GloMax Discover System (Promega) reader. The control cells showed a comparable level of *Renilla*-corrected firefly signal, whereas the fibroblasts from individuals 1 and 4 showed reduced firefly

activity, indicating a reduced matrix ATP content ([Figure 4C](#)).

Our findings strengthen the relation between SLC25A24 function and resistance to oxidative stress. The altered mitochondrial function in GCMS is consistent with findings in other syndromes with lipoatrophy.^{32,34} Interestingly, an association between SLC25A24 and fat-tissue

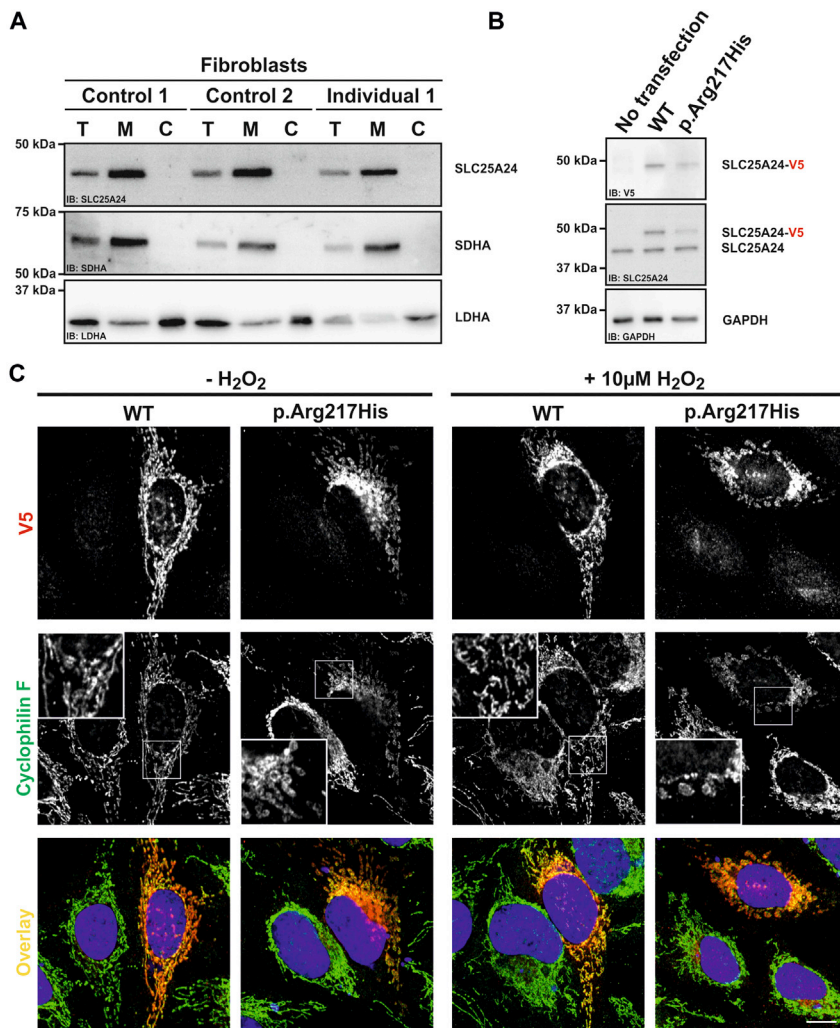


Figure 3. Mitochondrial Localization, Swelling, and Fragmentation of Mitochondria Harboring p.Arg217His SLC25A24

(A) A crude enrichment of mitochondria was performed from fibroblasts as previously described.³³ SLC25A24 was detectable in the total (T) cell lysates, and the intensity increased in the mitochondria-enriched fraction (M) in all fibroblast lines. The mitochondrial marker SDHA (Abcam) showed the same pattern, and neither protein was detectable in the cytosolic fraction (C). LDHA (Cell Signaling), a protein localized in the cytoplasm, was strongly reduced in the mitochondrial fraction. This experiment was performed twice with different cell lysates.

(B) Transient overexpression of V5-tagged WT and p.Arg217His SLC25A24 in HeLa cells. Compared with non-transfected cells, cells transiently transfected with WT and p.Arg217His SLC25A24 were detectable by a specific antibody against the V5 tag (Sigma). In all three lanes, the endogenous protein was detectable by an antibody against SLC25A24. Compared with the intrinsic SLC25A24, the transiently expressed V5-tagged proteins displayed an approximately 6 kDa band shift. This experiment was performed twice with different cell lysates.

(C) WT and p.Arg217His SLC25A24 both localized to mitochondria. Under normal culture conditions, expression of WT SLC25A24 had no impact on the mitochondrial structure. However, overexpression of p.Arg217His SLC25A24 caused swelling and partial fragmentation of mitochondria, which was further pronounced after treatment with 10 μ M H₂O₂ for 30 min. This experiment was performed four times. Scale bar, 10 μ m.

metabolism has been previously suggested by a genome-wide association study.³⁵ Furthermore, *Slc25a24* expression was increased in white adipose tissue under a high-fat diet in WT mice, and homozygous knockout (KO) of *Slc25a24* resulted in an obesity-resistant phenotype. KO of *Slc25a25*, a paralog of *Slc25a24*, caused lower cellular ATP levels, reduced physical endurance, and (as with the KO of *Slc25a24*) resistance to diet-induced obesity in mice.³⁶ *De novo* mutations in *SLC25A4* (MIM: 103220), encoding the mitochondrial ADP/ATP carrier, lead to a mitochondriopathy with reduced mtDNA copy number (MIM: 617184).³⁷ Although both proteins are related and functionally linked, and despite the accepted relationship between mtDNA mutations and progeroid symptoms,³⁸ the phenotypic differences and absence of mtDNA alterations in our probands hint at an unrelated pathomechanism.

Other studies have supposed an increased formation of the mPTP upon a reduced transport activity of SLC25A24.³⁰ Opening of the mPTP allows free passage of solutes up to 1.5 kDa in size and can cause the inner membrane potential to collapse, the respiratory chain to uncouple, and mitochondria to swell and rupture.^{31,39–41} In cells

expressing mutant SLC25A24, we found mitochondrial fragmentation and swelling, and the reduced ATP content measured in mutant cells could be explained by an opening of the mPTP. We therefore hypothesize that mPTP formation is enhanced by the mutant SLC25A24. Because Mg²⁺ has been shown to inhibit mPTP formation, this could be partially related to a lower ATP-Mg²⁺ content in mutant mitochondria as a result of decreased transport activity of SLC25A24.^{31,40} The higher membrane potential measured in mutant cells exposed to H₂O₂ might mirror an increased tendency to form hyperpolarized mitochondrial fragments, which has been described at moderate levels of oxidative stress.⁴² These hypotheses will be the subject of further research. We therefore assume that the amino acid changes p.Arg217His and p.Arg217Cys entail a gain of pathological function that interferes with the physiological SLC25A24 function regulating the mPTP.

Individuals with GCMS also present with coronal craniosynostosis. Growth of the cranial vault depends on an intricate balance between proliferation and differentiation of neural-crest-derived osteogenic stem cells in the sutures.⁴³ A lack of proliferation, an increase in cell death, or a premature osteogenic differentiation can lead to

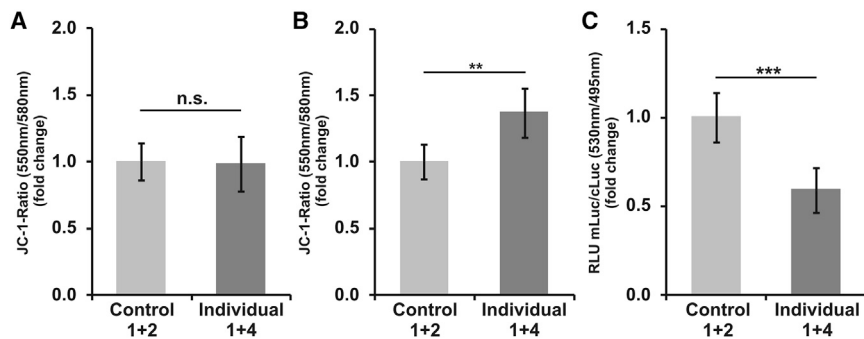


Figure 4. Altered Mitochondrial Function in Fibroblasts Carrying p.Arg217His

(A and B) Quantification of mitochondrial membrane potential (MMP) with JC-1. (A) Compared with control fibroblasts, fibroblasts from individuals 1 and 4 (cultured under standard conditions) showed no abnormality of the MMP. (B) However, after treatment with 25 μ M H₂O₂ for 18 min, the JC-1 signal ratio was higher in the probands' cells than in control cells (**p value < 0.005).

(C) Measurement of ATP content in the mitochondrial matrix. ATP-dependent firefly luciferase was fused to a COX8

targeting signal and thereby localized to this compartment after transient overexpression. Cytoplasmically targeted *Renilla* luciferase was transfected as a control. Compared with control cells, the fibroblasts from the affected individuals showed a decrease in firefly luminescence (***p value < 0.00001). All experiments were performed at least three times. Error bars represent SEM.

untimely closure of the sutures. Central regulators of this process are the fibroblast growth receptors and the transcriptional regulator TWIST1.⁴⁴ Dominant mutations leading to haploinsufficiency of *TWIST1* (MIM: 601622) are the cause of Saethre-Chotzen syndrome.^{45,46} Interestingly, the heterozygous KO of *Twist1* results in not only craniofacial defects, hindlimb polydactyly, and long-bone abnormalities but also obesity resistance in adult mice (similarly to homozygous *Slc25a24* KO).^{47,48} Different aspects of the *Twist1*-related phenotype were attributed to mitochondrial dysfunction leading to metabolic changes, uncoupling in brown adipose tissue, and altered cell death.^{48,49} Missense mutations in the sequence coding for the basic domain of TWIST2 (UniProt: Q8WVJ9), 98% identical to the basic domain of TWIST1 (UniProt: Q15672),⁵⁰ cause Barber-Say syndrome (MIM: 209885) and Ablepharon-Macrostomia syndrome (MIM: 200110).⁵¹ Both disorders show features overlapping those of GCMS, including hypertrichosis, a low frontal hair line, genital hypoplasia, maxillary hypoplasia, nail hypoplasia, and wrinkled, translucent skin, but not craniosynostosis. This indicates potential overlaps between TWIST signaling and SLC25A24 function.^{49,52–54}

In the accompanying article in this issue of *The American Journal of Human Genetics*, Witzl et al. report the same c.650G>A and c.649C>T mutations in *SLC25A24* but in association with Petty-type congenital progeroid syndrome, referred to as Fontaine syndrome.⁵⁵ Both phenotypes show overlapping clinical features (such as growth retardation, craniosynostosis, reduced subcutaneous fat, and small distal phalanges) but differ in some facial characteristics. The most striking difference is the early demise in Fontaine syndrome and a mostly normal lifespan in GCMS. However, two of the individuals reported here had severe failure to thrive, and their survival was probably dramatically improved by the medical intervention they received. We hypothesize that variations in the function of other genes involved in mitochondrial function, as well as other genetic, epigenetic, and environmental influences, could explain the variability of the phenotype.

In summary, we have identified recurrent *de novo* missense *SLC25A24* mutations affecting the same arginine residue in five girls with GCMS. Our findings of an increased sensitivity to oxidative stress of mutant cells *in vitro*, illustrated by mitochondrial swelling and a reduced ATP content, uncover a link between mitochondrial transporter function and a variable progeroid appearance due to changes in the development of skeletal, fat, and connective tissue. We assume that the *SLC25A24* mutations influence the formation or opening of the mPTP. The underlying molecular mechanisms and the impact of these findings on the development of skeletal and connective tissue will be the subject of future research.

Supplemental Data

Supplemental Data include a Supplemental Note, two figures, and two movies and can be found with this article online at <https://doi.org/10.1016/j.ajhg.2017.09.016>.

Acknowledgments

We would like to thank the families for their collaboration and contribution to this project. We thank Gabriele Hildebrand, Susanne Rothe, Catrin Janetzki, Esther Gill, and Gundula Leschik for excellent technical assistance. We thank Tori Pantel for helping with the design of figure layout and Dr. Peter N. Robinson for proof-reading. We want to thank Peter Meinecke for valuable advice. The plasmid containing the *SLC25A24* open reading frame was obtained from the DNASU Plasmid Repository (HsCD00296732). N.E. is a participant in the Berlin Institute of Health Charité Clinician Scientist Program, funded by the Charité – Universitätsmedizin Berlin and the Berlin Institute of Health. S.M. was supported by grants from the Deutsche Forschungsgemeinschaft (DFG) and the Max Planck Foundation, B.W. was supported by grants from the DFG SFB1002 project D02, and B.F.-Z. was supported by a grant from the DFG (FI 2240/1-1). U.K. received funding from FP7-EU grant agreement no. 602300 (SYBIL) and the DFG Research Unit FOR 2165 (249509554). Research reported in this publication was supported by National Institute of Neurological Disorders and Stroke of the National Institutes of Health under award number R01NS08372 to P.E.B.

Web Resources

Ensembl, <https://www.ensembl.org/index.html>
Exome Aggregation Consortium (ExAC) Browser, <http://exac.broadinstitute.org/>
GenBank, <https://www.ncbi.nlm.nih.gov/genbank/>
GeneTalk, <http://www.gene-talk.de/>
Genome Aggregation Database (GnomAD), <http://gnomad.broadinstitute.org/>
MGI Batch Query, <http://www.informatics.jax.org/batch>
Mutalyzer, <https://www.mutalyzer.nl/>
Mutation Taster, <http://www.mutationtaster.org/>
NCBI Conserved Domains, <http://www.ncbi.nlm.nih.gov/Structure/cdd/wrpsb.cgi>
NHLBI GO Exome Sequencing Project (ESP) Exome Variant Server, <http://evs.gs.washington.edu/EVS/>
OMIM, <http://www.omim.org>
PolyPhen-2, <http://genetics.bwh.harvard.edu/pph2/>
Protein BLAST, <http://www.ncbi.nlm.nih.gov/BLAST/Blast.cgi?PAGE=Proteins>
SIFT, http://sift.jcvi.org/www/SIFT_enst_submit.htm
UCSC Genome Browser, <https://genome.ucsc.edu/>
UniProt, <http://www.uniprot.org/>

References

1. Gorlin, R.J., Chaudhry, A.P., and Moss, M.L. (1960). Craniofacial dysostosis, patent ductus arteriosus, hypertrichosis, hypoplasia of labia majora, dental and eye anomalies—a new syndrome? *J. Pediatr.* *56*, 778–785.
2. Aravena, T., Passalacqua, C., Pizarro, O., and Aracena, M. (2011). Two sisters resembling Gorlin-Chaudhry-Moss syndrome. *Am. J. Med. Genet. A.* *155A*, 2552–2555.
3. Preis, S., Kaewel, E.V., and Majewski, F. (1995). Gorlin-Chaudhry-Moss or Saethre-Chotzen syndrome? *Clin. Genet.* *47*, 267–269.
4. Ippel, P.F., Gorlin, R.J., Lenz, W., van Doorne, J.M., and Bijlsma, J.B. (1992). Craniofacial dysostosis, hypertrichosis, genital hypoplasia, ocular, dental, and digital defects: confirmation of the Gorlin-Chaudhry-Moss syndrome. *Am. J. Med. Genet.* *44*, 518–522.
5. Adolphs, N., Klein, M., Haberl, E.J., Graul-Neumann, L., Meneking, H., and Hoffmeister, B. (2011). Necrotizing soft tissue infection of the scalp after fronto-facial advancement by internal distraction in a 7-year old girl with Gorlin-Chaudhry-Moss syndrome—a case report. *J. Craniomaxillofac. Surg.* *39*, 554–561.
6. Rosti, R.O., Karaer, K., Karaman, B., Torun, D., Guran, S., and Bahce, M. (2013). Gorlin-Chaudhry-Moss syndrome revisited: expanding the phenotype. *Am. J. Med. Genet. A.* *161A*, 1737–1742.
7. Cohen, M.M., Jr. (1975). An etiologic and nosologic overview of craniosynostosis syndromes. *Birth Defects Orig. Artic. Ser.* *11*, 137–189.
8. Castori, M., Silvestri, E., Pedace, L., Marseglia, G., Tempera, A., Antignoni, I., Torricelli, F., Majore, S., and Grammatico, P. (2009). Fontaine-Farriaux syndrome: a recognizable craniosynostosis syndrome with nail, skeletal, abdominal, and central

- nervous system anomalies. *Am. J. Med. Genet. A.* *149A*, 2193–2199.
9. Li, H. (2013). Aligning sequence reads, clone sequences and assembly contigs with BWA-MEM. arXiv, arXiv:1303.3997v2, <https://arxiv.org/abs/1303.3997>.
 10. DePristo, M.A., Banks, E., Poplin, R., Garimella, K.V., Maguire, J.R., Hartl, C., Philippakis, A.A., del Angel, G., Rivas, M.A., Hanna, M., et al. (2011). A framework for variation discovery and genotyping using next-generation DNA sequencing data. *Nat. Genet.* *43*, 491–498.
 11. Heinrich, V., Kamphans, T., Stange, J., Parkhomchuk, D., Hecht, J., Dickhaus, T., Robinson, P.N., and Krawitz, P.M. (2013). Estimating exome genotyping accuracy by comparing to data from large scale sequencing projects. *Genome Med.* *5*, 69.
 12. Jäger, M., Wang, K., Bauer, S., Smedley, D., Krawitz, P., and Robinson, P.N. (2014). Jannovar: a java library for exome annotation. *Hum. Mutat.* *35*, 548–555.
 13. Kamphans, T., and Krawitz, P.M. (2012). GeneTalk: an expert exchange platform for assessing rare sequence variants in personal genomes. *Bioinformatics* *28*, 2515–2516.
 14. Abecasis, G.R., Auton, A., Brooks, L.D., DePristo, M.A., Durbin, R.M., Handsaker, R.E., Kang, H.M., Marth, G.T., McVean, G.A.; and 1000 Genomes Project Consortium (2012). An integrated map of genetic variation from 1,092 human genomes. *Nature* *491*, 56–65.
 15. Lek, M., Karczewski, K.J., Minikel, E.V., Samocha, K.E., Banks, E., Fennell, T., O'Donnell-Luria, A.H., Ware, J.S., Hill, A.J., Cummings, B.B., et al.; Exome Aggregation Consortium (2016). Analysis of protein-coding genetic variation in 60,706 humans. *Nature* *536*, 285–291.
 16. Hussain, M.S., Battaglia, A., Szczepanski, S., Kaygusuz, E., Tolia, M.R., Sakakibara, S., Altmüller, J., Thiele, H., Nürnberg, G., Moosa, S., et al. (2014). Mutations in CKAP2L, the human homolog of the mouse Radmis gene, cause Filippi syndrome. *Am. J. Hum. Genet.* *95*, 622–632.
 17. Keupp, K., Beleggia, F., Kayserili, H., Barnes, A.M., Steiner, M., Semler, O., Fischer, B., Yigit, G., Janda, C.Y., Becker, J., et al. (2013). Mutations in WNT1 cause different forms of bone fragility. *Am. J. Hum. Genet.* *92*, 565–574.
 18. Besse, A., Wu, P., Bruni, F., Donti, T., Graham, B.H., Craigen, W.J., McFarland, R., Moretti, P., Lalani, S., Scott, K.L., et al. (2015). The GABA transaminase, ABAT, is essential for mitochondrial nucleoside metabolism. *Cell Metab.* *21*, 417–427.
 19. Stiles, A.R., Ferdinandusse, S., Besse, A., Appadurai, V., Leydiker, K.B., Cambray-Forker, E.J., Bonnen, P.E., and Abdenur, J.E. (2015). Successful diagnosis of HIBCH deficiency from exome sequencing and positive retrospective analysis of newborn screening cards in two siblings presenting with Leigh's disease. *Mol. Genet. Metab.* *115*, 161–167.
 20. Heinrich, V., Kamphans, T., Mundlos, S., Robinson, P.N., and Krawitz, P.M. (2017). A likelihood ratio based method to predict exact pedigrees for complex families from next-generation sequencing data. *Bioinformatics* *33*, 72–78.
 21. Schwarz, J.M., Rödelsperger, C., Schuelke, M., and Seelow, D. (2010). MutationTaster evaluates disease-causing potential of sequence alterations. *Nat. Methods* *7*, 575–576.
 22. Kumar, P., Henikoff, S., and Ng, P.C. (2009). Predicting the effects of coding non-synonymous variants on protein function using the SIFT algorithm. *Nat. Protoc.* *4*, 1073–1081.
 23. Adzhubei, I., Jordan, D.M., and Sunyaev, S.R. (2013). Predicting functional effect of human missense mutations using PolyPhen-2. *Curr. Protoc. Hum. Genet.* *Chapter 7*, 20.

24. Lorenz, C., Lesimple, P., Bukowiecki, R., Zink, A., Inak, G., Mlody, B., Singh, M., Semtner, M., Mah, N., Auré, K., et al. (2017). Human iPSC-Derived Neural Progenitors Are an Effective Drug Discovery Model for Neurological mtDNA Disorders. *Cell Stem Cell* 20, 659–674.e9.
25. del Arco, A., and Satrustegui, J. (2004). Identification of a novel human subfamily of mitochondrial carriers with calcium-binding domains. *J. Biol. Chem.* 279, 24701–24713.
26. Run, C., Yang, Q., Liu, Z., OuYang, B., and Chou, J.J. (2015). Molecular Basis of MgATP Selectivity of the Mitochondrial SCaMC Carrier. *Structure* 23, 1394–1403.
27. Aprille, J.R. (1993). Mechanism and regulation of the mitochondrial ATP-Mg/P(i) carrier. *J. Bioenerg. Biomembr.* 25, 473–481.
28. Yang, Q., Brüscheweiler, S., and Chou, J.J. (2014). A self-sequestered calmodulin-like Ca²⁺ sensor of mitochondrial SCaMC carrier and its implication to Ca²⁺-dependent ATP-Mg/P(i) transport. *Structure* 22, 209–217.
29. Harborne, S.P., King, M.S., Crichton, P.G., and Kunji, E.R. (2017). Calcium regulation of the human mitochondrial ATP-Mg/Pi carrier SLC25A24 uses a locking pin mechanism. *Sci. Rep.* 7, 45383.
30. Traba, J., Del Arco, A., Duchen, M.R., Szabadkai, G., and Satrustegui, J. (2012). SCaMC-1 promotes cancer cell survival by desensitizing mitochondrial permeability transition via ATP/ADP-mediated matrix Ca(2+) buffering. *Cell Death Differ.* 19, 650–660.
31. Kwong, J.Q., and Molkentin, J.D. (2015). Physiological and pathological roles of the mitochondrial permeability transition pore in the heart. *Cell Metab.* 21, 206–214.
32. Reversade, B., Escande-Beillard, N., Dimopoulou, A., Fischer, B., Chng, S.C., Li, Y., Shboul, M., Tham, P.Y., Kayserili, H., Al-Gazali, L., et al. (2009). Mutations in PYCR1 cause cutis laxa with progeroid features. *Nat. Genet.* 41, 1016–1021.
33. Hartmann, B., Wai, T., Hu, H., MacVicar, T., Musante, L., Fischer-Zirnsak, B., Stenzel, W., Gräf, R., van den Heuvel, L., Ropers, H.H., et al. (2016). Homozygous YME1L1 mutation causes mitochondriopathy with optic atrophy and mitochondrial network fragmentation. *eLife* 5, 5.
34. Fischer-Zirnsak, B., Escande-Beillard, N., Ganesh, J., Tan, Y.X., Al Bughaili, M., Lin, A.E., Sahai, I., Bahena, P., Reichert, S.L., Loh, A., et al. (2015). Recurrent De Novo Mutations Affecting Residue Arg138 of Pyrroline-5-Carboxylate Synthase Cause a Progeroid Form of Autosomal-Dominant Cutis Laxa. *Am. J. Hum. Genet.* 97, 483–492.
35. Urano, T., Shiraki, M., Sasaki, N., Ouchi, Y., and Inoue, S. (2015). SLC25A24 as a novel susceptibility gene for low fat mass in humans and mice. *J. Clin. Endocrinol. Metab.* 100, E655–E663.
36. Anunciado-Koza, R.P., Zhang, J., Ukropec, J., Bajpeyi, S., Koza, R.A., Rogers, R.C., Cefalu, W.T., Mynatt, R.L., and Kozak, L.P. (2011). Inactivation of the mitochondrial carrier SLC25A25 (ATP-Mg²⁺/Pi transporter) reduces physical endurance and metabolic efficiency in mice. *J. Biol. Chem.* 286, 11659–11671.
37. Thompson, K., Majd, H., Dallabona, C., Reinson, K., King, M.S., Alston, C.L., He, L., Lodi, T., Jones, S.A., Fattal-Valevski, A., et al. (2016). Recurrent De Novo Dominant Mutations in SLC25A4 Cause Severe Early-Onset Mitochondrial Disease and Loss of Mitochondrial DNA Copy Number. *Am. J. Hum. Genet.* 99, 860–876.
38. Ahlqvist, K.J., Hämäläinen, R.H., Yatsuga, S., Uutela, M., Terzioglu, M., Götz, A., Forsström, S., Salven, P., Angers-Loustau, A., Kopra, O.H., et al. (2012). Somatic progenitor cell vulnerability to mitochondrial DNA mutagenesis underlies progeroid phenotypes in Polg mutator mice. *Cell Metab.* 15, 100–109.
39. Hunter, D.R., and Haworth, R.A. (1979). The Ca²⁺-induced membrane transition in mitochondria. III. Transitional Ca²⁺ release. *Arch. Biochem. Biophys.* 195, 468–477.
40. Hunter, D.R., and Haworth, R.A. (1979). The Ca²⁺-induced membrane transition in mitochondria. I. The protective mechanisms. *Arch. Biochem. Biophys.* 195, 453–459.
41. Haworth, R.A., and Hunter, D.R. (1979). The Ca²⁺-induced membrane transition in mitochondria. II. Nature of the Ca²⁺ trigger site. *Arch. Biochem. Biophys.* 195, 460–467.
42. Menges, S., Minakaki, G., Schaefer, P.M., Meixner, H., Prots, I., Schlötzer-Schrehardt, U., Friedland, K., Winner, B., Outeiro, T.F., Winklhofer, K.F., et al. (2017). Alpha-synuclein prevents the formation of spherical mitochondria and apoptosis under oxidative stress. *Sci. Rep.* 7, 42942.
43. Twigg, S.R., and Wilkie, A.O. (2015). A Genetic-Pathophysiological Framework for Craniosynostosis. *Am. J. Hum. Genet.* 97, 359–377.
44. Ornitz, D.M., and Marie, P.J. (2015). Fibroblast growth factor signaling in skeletal development and disease. *Genes Dev.* 29, 1463–1486.
45. el Ghouzzi, V., Le Merrer, M., Perrin-Schmitt, F., Lajeunie, E., Benit, P., Renier, D., Bourgeois, P., Bolcato-Bellemin, A.L., Munnich, A., and Bonaventure, J. (1997). Mutations of the TWIST gene in the Saethre-Chotzen syndrome. *Nat. Genet.* 15, 42–46.
46. Howard, T.D., Paznekas, W.A., Green, E.D., Chiang, L.C., Ma, N., Ortiz de Luna, R.I., Garcia Delgado, C., Gonzalez-Ramos, M., Kline, A.D., and Jabs, E.W. (1997). Mutations in TWIST, a basic helix-loop-helix transcription factor, in Saethre-Chotzen syndrome. *Nat. Genet.* 15, 36–41.
47. Bourgeois, P., Bolcato-Bellemin, A.L., Danse, J.M., Bloch-Zupan, A., Yoshida, K., Stoetzel, C., and Perrin-Schmitt, F. (1998). The variable expressivity and incomplete penetrance of the twist-null heterozygous mouse phenotype resemble those of human Saethre-Chotzen syndrome. *Hum. Mol. Genet.* 7, 945–957.
48. Pan, D., Fujimoto, M., Lopes, A., and Wang, Y.X. (2009). Twist-1 is a PPARdelta-inducible, negative-feedback regulator of PGC-1alpha in brown fat metabolism. *Cell* 137, 73–86.
49. Connerney, J., Andreeva, V., Leshem, Y., Mercado, M.A., Dowell, K., Yang, X., Lindner, V., Friesel, R.E., and Spicer, D.B. (2008). Twist1 homodimers enhance FGF responsiveness of the cranial sutures and promote suture closure. *Dev. Biol.* 318, 323–334.
50. Franco, H.L., Casasnovas, J., Rodríguez-Medina, J.R., and Cadilla, C.L. (2011). Redundant or separate entities?—roles of Twist1 and Twist2 as molecular switches during gene transcription. *Nucleic Acids Res.* 39, 1177–1186.
51. Marchegiani, S., Davis, T., Tessadori, F., van Haften, G., Brancati, F., Hoischen, A., Huang, H., Valkanas, E., Pusey, B., Schanze, D., et al. (2015). Recurrent Mutations in the Basic Domain of TWIST2 Cause Ablepharon Macrostomia and Barber-Say Syndromes. *Am. J. Hum. Genet.* 97, 99–110.
52. Hayashi, M., Nimura, K., Kashiwagi, K., Harada, T., Takaoka, K., Kato, H., Tamai, K., and Kaneda, Y. (2007). Comparative roles of Twist-1 and Id1 in transcriptional regulation by BMP signaling. *J. Cell Sci.* 120, 1350–1357.

53. Reinhold, M.I., Kapadia, R.M., Liao, Z., and Naski, M.C. (2006). The Wnt-inducible transcription factor Twist1 inhibits chondrogenesis. *J. Biol. Chem.* *281*, 1381–1388.
54. Bialek, P., Kern, B., Yang, X., Schrock, M., Sobic, D., Hong, N., Wu, H., Yu, K., Ornitz, D.M., Olson, E.N., et al. (2004). A twist code determines the onset of osteoblast differentiation. *Dev. Cell* *6*, 423–435.
55. Witzl, K., Maver, A., Kovacic, L., Martinez-Valero, P., Contreras, L., Satrustegui, J., Castori, M., Faivre, L., Lapunzina, P., van Kuilenburg, A.B.P., et al. (2017). De Novo Mutations in SLC25A24 Cause a Disorder Characterized by Early Aging, Bone Dysplasia, and Characteristic Face, and Early Demise. *Am. J. Hum. Genet.* *101*, this issue, 844–855.